Journal of Controlled Release 329 (2021) 361–371

Contents lists available at ScienceDirect

Journal of Controlled Release

journal homepage: www.elsevier.com/locate/jconrel

Synthetic high-density lipoproteins delivering liver X receptor agonist prevent atherogenesis by enhancing reverse cholesterol transport

Wenmin Yuan [a,1], Bilian Yu [b,e,1], Minzhi Yu [a], Rui Kuai [a,f], Emily E. Morin [a], Huilun Wang [b], Die Hu [b], Jifeng Zhang [b], James J. Moon [a,c,d], Y. Eugene Chen [b], Yanhong Guo [b,**], Anna Schwendeman [a,c,*]

[a] Department of Pharmaceutical Sciences, University of Michigan, Ann Arbor, MI 48109, United States
[b] Department of Internal Medicine, University of Michigan, Ann Arbor, MI 48109, United States
[c] Biointerfaces Institute, University of Michigan, Ann Arbor, MI 48109, United States
[d] Department of Biomedical Engineering, University of Michigan, Ann Arbor, MI 48109, United States
[e] Department of Cardiovascular medicine, The Second Xiangya Hospital, Central South University, Changsha, Hunan, China
[f] School of Pharmaceutical Sciences, Tsinghua University, Beijing, China

ARTICLE INFO

Keywords:
Liver X receptors
Synthetic high-density lipoprotein
Atherosclerosis
Atheroma targeting
Reverse cholesterol transport

ABSTRACT

Liver X nuclear receptor (LXR) agonists are promising anti-atherosclerotic agents that increase the expression of cholesterol transporters on atheroma macrophages leading to increased efflux of cholesterol to endogenous high-density lipoprotein (HDL) acceptors. HDL subsequently delivers effluxed cholesterol to the liver by the process of reverse cholesterol transport, resulting in reduction of atherosclerotic plaques. However, LXR agonists administration triggers undesirable liver steatosis and hypertriglyceridemia due to increased fatty acid and sterol synthesis. LXR-induced liver toxicity, poor drug aqueous solubility and low levels of endogenous HDL acceptors in target patient populations limit the clinical translation of LXR agonists. Here, we propose a dual-antiatherogenic strategy for administration of the LXR agonist, T0901317 (T1317), by encapsulating in synthetic HDL (sHDL) nanoparticles. sHDL had been clinically proven to serve as cholesterol acceptors, resulting in plaque reduction in atherosclerosis patients. In addition, the hydrophobic core and endogenous atheroma-targeting ability of sHDL allow for encapsulation of water-insoluble drugs and their subsequent delivery to atheroma. Several compositions of sHDL were tested to optimize both T1317 encapsulation efficiency and ability of T1317-sHDL to efflux cholesterol. Optimized T1317-sHDL exhibited more efficient cholesterol efflux from macrophages and enhanced atheroma-targeting relative to free drug. Most importantly, in an apolipoprotein E deficient ($ApoE^{-/-}$) atherosclerosis progression murine model, T1317-sHDL showed superior inhibition of atherogenesis and reduced hypertriglyceridemia side effects in comparison to the free drug and blank sHDL. The T1317-sHDL pharmacological efficacy was observed at doses lower than those previously described for LXR agents, which may have additional safety benefits. In addition, the established clinical manufacturing, safety and efficacy of blank sHDL nanoparticles used in this study could facilitate future clinical translation of LXR-loaded sHDLs.

1. Introduction

Liver X receptor (LXR) agonists are lipid metabolism regulators that have been used for the treatment of atherosclerosis, diabetes and Alzheimer's disease in animal models and clinical trials [1–4]. LXR agonists upregulate expression of ATP-binding cassette transporters from subfamilies A1 and G1 (ABCA1 and ABCG1), which are responsible for effluxing excess cholesterol from cells, such as atheroma macrophages, to high density lipoprotein (HDL) particles [5,6]. The HDL particles subsequently deliver effluxed cholesterol to the liver for elimination by utilizing the endogenous reverse cholesterol transport (RCT) pathway [7]. Due to the increased cholesterol efflux from atheroma macrophages,

* Corresponding author at: Department of Pharmaceutical Sciences, University of Michigan, Ann Arbor, MI 48109, United States.
** Corresponding author.
E-mail addresses: yanhongg@umich.edu (Y. Guo), annaschw@med.umich.edu (A. Schwendeman).
[1] Denote equal contribution.

https://doi.org/10.1016/j.jconrel.2020.11.016
Received 27 March 2019; Received in revised form 22 October 2020; Accepted 8 November 2020
Available online 11 November 2020

administration of LXR agonists has been shown to reduce existing plaque burden in ApoE$^{-/-}$ murine models of atherosclerosis [8–10].

A number of LXR agonists were advanced to clinical development for the treatment of atherosclerosis, but their progress was hindered by hepatic side effects [11–13]. In the liver, LXR agonists activate lipogenesis by upregulation of sterol regulatory element-binding transcription factor 1c (SREBP-1c) gene expression, resulting in hepatic steatosis and secretion of excess of triglycerides into systemic circulation [13,14]. This secretion leads to an elevated plasma levels of very low-density lipoproteins (VLDL), which is convert in the bloodstream to low-density lipoprotein (LDL) and intermediate-density lipoprotein (IDL), known to be pro-atherogenic [11]. Such drug-associated liver toxicity was observed in animal models because of the high doses of LXR agonists (10–50 mg/kg) required to obtain anti-atherosclerotic effects [10,13,15–19].

For the past two decades, sHDL nanoparticles have been designed and clinically developed for treatment of atherosclerosis [20,21]. Those sHDL mimic the structure and function of a specific sub-fraction of endogenous HDL particles, called pre-β HDL. Only 2–5% of all endogenous HDL are classified as pre-β based on its electrophoretic mobility and discoidal shape [22]. Clinically tested synthetic pre-β HDL products consist of lipid bilayers wrapped around by either full-length apolipoprotein A-I (apoA-I) [23–25] or apoA-I synthetic peptide (ETC-642) [26] to form nanodisc structures with diameters of 8–12 nm. Due to their small size, pre-β HDL are capable of accumulating in the atheroma area where they efflux the excess of cholesterol from cholesterol-laden macrophages and, subsequently, deliver to the liver for elimination [7,22]. Acute treatment consisting of 4–6 weekly infusion of sHDL has been shown to reduce plaque burden in coronary artery disease patients [25,27,28].

In this research, we hypothesize that the intrinsic atheroma targeting property of sHDL can be exploited for efficient delivery of an LXR agonist, T0901317 (T1317), to lipid-laden atheroma macrophages, where the LXR agonist can upregulate expression of ABCA1/G1 and facilitate efflux of cellular cholesterol. Once the sHDL has accomplished atheroma targeted LXR delivery, the sHDL can accept effluxed cholesterol from the macrophages, as it has demonstrated in the clinic [23–26]. Previously, to test this hypothesis, we demonstrated that T1317-sHDL nanoparticles are capable of atheroma regression in a severe model of atherosclerosis [29]. T1317-sHDL were able to deliver LXR agonist to atheroma *in vivo* where it upregulated expression of ABCA1/G1.

In the current study, we report the original formulation optimization of the novel T1317-sHDL in order to maximize the dual nanoparticle action as a targeting drug delivery agent and as acceptor of cholesterol. Secondly, we further tested our hypothesis by exploring the capability of T1317-sHDL to halt development of atherosclerotic lesions using an early onset plaque formation ApoE$^{-/-}$ murine atherogenesis model. Hence, this approach has the potential to expand the capability and potency of T1317-sHDL for halting development and treating atherosclerosis.

2. Materials and methods

2.1. Reagents

ApoA-I mimetic peptide 22A with the ends uncapped, PVLDLFRELLNELLEALKQKLK, was synthesized by Genscript Inc. (Piscataway, NJ). 1-palmitoyl-2-oleoyl-*sn*-glycero-3-phosphocholine (POPC), 1,2-dimyristoyl-*sn*-glycero-3-phosphocholine (DMPC), 1,2-dipalmitoyl-*sn*-glycero-3-phosphocholine (DPPC), egg sphingomyelin (eSM) were purchased from NOF America Corporation (White Plains, NY). Fluorescent dye DiD (1,1′-dioctadecyl-3,3,3′,3′-tetramethylindodicarbocyanine perchlorate) was purchased from Invitrogen Corporation (Carlsbad, CA). LXR receptor agonist, T0901317 (T1317) was purchased from Cayman Chemical (Ann Arbor, MI). All other materials were obtained from commercial sources.

2.2. Preparation of sHDL nanoparticles

All sHDL were prepared by the lyophilization method [30,31]. To prepare T1317-loaded sHDL, a predetermined amount of lipids and 22A dissolved in glacial acetic acid and T1317 dissolved in methanol were mixed and freeze-dried overnight. The freeze-dried mixture was hydrated with PBS (pH 7.4). The suspension was thermal cycled 3 times above and below the lipid's transition temperature and probe-sonicated (1w × 1 min) after the 1st and 2nd thermal cycle. The pH of sHDL solution was adjusted to 7.4 with NaOH. The T1317-sHDL were prepared with a 1:1 to 1:4 w/w ratio of 22A peptide to phospholipids and contained 1.25 to 5.0% of theoretical loading of T1317 to phospholipids. The DiD-loaded sHDL (0.2 mol%) were prepared similarly to T1317-sHDL except that DiD was dissolved in chloroform.

2.3. Characterization of sHDL

The size distributions of sHDL were analyzed by dynamic light scattering (DLS). All sHDL were directly diluted by PBS to a concentration of 3 mg/mL 22A before measurement by Malvern Zetasizer Nano ZS.

The homogeneity and purity of sHDL were analyzed by gel permeation chromatography (GPC). sHDL samples were diluted by PBS to a concentration of 1 mg/mL 22A and centrifuged at 12,500 rpm for 10 min at RT. 25 μL of the supernatant was analyzed by GPC on a Tosoh TSK gel G3000SWxl column with UV detection at 220 nm. The mobile phase, PBS, was delivered at an isocratic flow rate of 1 mL/min.

The morphology of sHDL was observed by transmission electron microscopy (TEM). sHDL samples were diluted with 20 mM Tris/HCl (pH 7.5) to a 22A concentration of 6 μg/mL, and 3.5 μL of diluted sHDL were adsorbed on glow-discharged G400-Cu thin-carbon-coated copper grids (400 mesh grid, electron microscopy sciences) and immediately negatively stained with 1% (w/v) uranyl formate solution. All specimens were imaged on a 100 kV Morgagni TEM equipped with a 2 K × 2 K Gatan Orius CCD.

The encapsulation efficiency of T1317-sHDL was detected using a desalting column (Thermo Scientific™ Zeba™ spin desalting columns, 7 K MWCO, with 0.5 mL resin) to remove the un-encapsulated T1317. T1317-sHDL samples (3 mg/mL) were centrifuged at 12,500 rpm for 10 min at RT to remove un-encapsulated T1317 precipitate, and 120 μL of the supernatant passed through the desalting column. The sHDL recovery from the desalting column was analyzed by GPC, and the concentration of T1317 in sHDL before and after desalting was quantified by UPLC-UV. The UPLC was performed on Waters® ACQUITY UPLC H-Class system equipped with a Waters® ACQUITY UPLC® BEH C18 column (2.1 mm × 50 mm, 1.7 μm) with UV detection at 220 nm. The sHDL samples were diluted 4 times by methanol and 5 μL injection volume was used. Sample was eluted with mobile phase of 70% MeOH (0.1% v/v TFA) with 30% water (0.1% v/v TFA) delivered at a flow rate as 0.5 mL/min. The T1317 encapsulation efficiency (%) was calculated from the ratio of drug concentration after and before desalting with normalization for sHDL recovery from the desalting step.

2.4. T1317 in vitro release assay

T1317-sHDL were diluted by PBS containing 0.02% (w/v) NaN_3 (pH 7.4) to a 22A concentration of 1 mg/mL. An 8 mL sample of diluted sHDL was combined with 400 mg Bio-Beads™ SM-2 adsorbent (Bio-Rad Laboratories) and incubated at 37 °C with rotation at 20 r.p.m. The Bio-Beads™ SM-2 adsorbed 100% of released T1317 within 10 min, thus, assuring sink release condition. At different time points, 30 μL aliquots were removed and concentrations of T1317 and lipid were analyzed by UPLC-MS. The UPLC-MS was performed using Waters® ACQUITY UPLC H-Class system equipped with an QDa Detector, and Waters® ACQUITY

UPLC® BEH300 C4 column (2.1 mm × 150 mm, 1.7 μm). sHDL samples were diluted 400 times by methanol and 1.5 μL was injected on the UPLC-MS. The mobile phase, delivered at a flow rate of 0.3 mL/min, was composed of (A) water (0.1% v/v formic acid), (B) acetonitrile (0.1% v/v formic acid) and (C) methanol (0.1% v/v formic acid) with gradient elution of A:B:C of 50:33:17 to 0:67:33 during 0–2.5 min, isocratic elution 0.5–4.2 min, gradient of A:B:C of 0:67:33 to 50:33:17 during 4.5–5 min and isocratic elution 5–8 min. The components were detected at the following masses: T1317 480.18 (−) (M-H); POPC 760.74 (+) (M + H); DMPC 678.72 (+) (M + H); DPPC 734.79 (+) (M + H); eSM 703.79 (+) (M + H). The sHDL recovery at each timepoint was calculated by analysis of lipid concentration. The percent of drug retained in sHDL at each time point was reported after correction for sHDL recovery.

2.5. In vitro serum remodeling

T1317-sHDL (22A concentration of 10 mg/mL) was incubated with fresh serum from normal C57 mice (1/1, v/v) for 8 h at 37 °C. At 0 and 8 h post incubation, 50 μL blank serum control or incubation mixtures were separated on a Superose™ 6, 10/300 GL column (GE Healthcare) and a WATERS® Fraction Collector III. Dual UV detection wavelengths were used to locate HDL, LDL and VLDL endogenous lipoproteins (UV 265 nm) and sHDL (UV 220 nm). The mobile phase 154 mM NaCl with 0.02% NaN_3 (w/v) was delivered with a flow rate of 1 mL/min. Post-column elution fractions were collected every 0.5 min from 7.5–19 min. Elution fraction samples were diluted 4 times by methanol prior to T1317 quantification by UPLC-MS by mass detection at 504.4 (+) (M + Na).

2.6. Cholesterol efflux assay

Cholesterol efflux studies were performed, as described previously [32]. Murine J774.1 macrophages (ATCC, Manassas, VA) were seeded in 48-well plates for 24 h. Cells were labeled with 1 μCi/mL [1,2−^{3}H]-cholesterol (Perkin Elmer, USA) in DMEM (Life Technologies Corp.) containing 0.3% fatty acid-free bovine serum albumin (BSA) and 5 μg/mL ACAT inhibitor Sandoz 58–035 (Sigma) overnight. To compare cholesterol efflux ability of different formulations of blank sHDL, the cells were treated with blank-sHDL (at 50 μg/mL 22A) for 8 h. The medium was then collected and filtered to remove detached cells. Results are expressed as fraction of total [^{3}H] cholesterol released into the medium (media counts/(media counts + cells counts) × 100%).

To detect the dual effect of T1317-sHDL on cholesterol efflux, after [1,2-^{3}H]-cholesterol-labelling, the cells were incubated with DMSO, T1317 at 0.1 μM, sHDL at 10 μg/mL 22A, or sHDL-T1317 (sHDL at 10 μg/mL 22A and T1317 at 0.1 μM, lower sHDL to delivery T1317) overnight. After removing the old medium, cells were incubated with fresh DMEM/BSA containing human HDL at 50 μg/mL (Sigma) or human ApoA-I (10 μg/mL) as acceptors for 5 h. The medium was then collected and filtered to remove detached cells and efflux was quantified by liquid scintillation. Percent of effluxed [^{3}H]-cholesterol was quantified by liquid scintillation.

2.7. RNA isolation and RT-PCR

Total RNA was purified using QIAGEN's RNeasy kits (QIAGEN). cDNA was synthesized using SuperScript III (Invitrogen), and qPCR was performed using SYBR green reagents (Bio-Rad). Primer pairs for reverse-transcriptase PCR (RT-PCR) are shown in Supplemental Table 1. Gene expression was presented as fold increase compared with RNA isolated from the control group by the comparative C_T ($2^{-\Delta\Delta CT}$) method with 18S RNA as the reference gene.

2.8. Protein extracts and Western blot

Cell extracts were prepared with RIPA lysis buffer that included the following: 25 mM Tris-HCl pH 7.6, 150 mM NaCl, 1% NP 40, 1% sodium deoxycholate, 0.1% SDS, and a protease inhibitor mixture (Roche). Protein extracts were resolved by SDS PAGE using 7% gels and electroblotted onto PVDF membranes (Bio-Rad). After blocking, membranes were incubated overnight with antibodies against ABCA1 (1:2000 from Abcam #ab18180) and β-Actin (1:3000 from Cell Signaling Technology mAb #3700) followed by a donkey anti-mouse IRDye-conjugated IgG (Li-Cor Odyssey) secondary antibody diluted 1:3000 for 1 h. Blots were scanned and the images displayed in grayscale (Li-Cor Odyssey).

2.9. Synthetic HDL nanoparticle mediated delivery of DiD to macrophages in vitro

The sHDL nanoparticles were labeled with a lipophilic fluorescent dye DiD using the same preparation method described above. THP-1 cells, a human monocytic cell line, were treated with 100 ng/mL phorbol 12-myristate 13-acetate (PMA, Sigma–Aldrich) to induce macrophage differentiation. Then the cells were treated with sHDL-DiD in serum-free DMEM for indicated lengths of time. Hoechst 33342 (Thermo Fisher) was added into the medium to stain nuclei. After washed with Dulbecco's phosphate-buffered saline (D-PBS), the cells were fixed with 4% paraformaldehyde and analyzed using a Nikon A-1 spectral confocal microscope system (Nikon Corporation, Tokyo). Quantification of cellular fluorescent signal was performed using a flow cytometer (Beckman Coulter FC500 5-color analyzer).

2.10. Atherogenesis study

ApoE-deficient mice were purchased from the Jackson Laboratories and were housed at 22 ± 1 °C in a 12:12-h light-dark cycle. All animal work was performed in accordance with the guidelines set by the University of Michigan Animal Care and Use Committee. Atherosclerosis studies were conducted as described [32].

2.10.1. Fluorescence microscopy analysis of atherosclerotic plaques

Mouse atherosclerotic models were generated by feeding 8-week-old male ApoE-deficient mice an atherogenic diet (high fat high cholesterol diet, HFHC diet, 21% fat, 34% sucrose, and 0.2% cholesterol, Harlan, T. D. 88,137) for 14 weeks. Mice received a single intraperitoneal injection consisting of 0.2 mL of sHDL-DiD (sHDL at 30 mg/kg 22A concentration and DiD at 200 μg/kg dose, respectively). Animals were sacrificed 4 h after injection, and brachiocephalic arteries including the atherosclerotic plaque were harvested under a microscope after they were perfused with PBS. Arteries from mice were fixed with 4% paraformaldehyde and then embedded in OCT (optimal cutting temperature). The cryostat sections of tissue (8 μm) were incubated with rat anti-mouse CD68 primary antibody (ThermoFisher, MA5-16674 1:100 dilution) for 1 h, followed by biotinylated rabbit anti-rat antibody (Vectorlabs, 1:200 dilution) and VECTASTAIN ABC-HRP kit (Vectorlabs). Images were obtained with an Olympus IX73 microscope.

2.10.2. Atherogenesis study

Mouse atherogenesis model was generated by feeding 8-week-old male ApoE-deficient mice placed on HFHC diet for 6 weeks. Mice were randomized into 5 groups and received IP injection three times a week (Monday, Wednesday, and Friday) of DMSO, T1317, PBS, sHDL, sHDL-T1317 (sHDL at 30 mg/kg and T1317 at 1.5 mg/kg) simultaneously with HFHC diet challenge. At the end of the study, the mice were anesthetized and subjected to whole-body perfusion to fix the tissues. The entire aorta was micro-dissected from each mouse. Atherosclerotic burden was quantified by measuring the surface area of Oil Red O positive lesions on *en* face preparations of whole aortas as previously described [32]. Aortas from the iliac bifurcation to the aortic root were excised and the adventitia was removed. After stained with Oil Red O (Sigma-Aldrich), aortas were opened longitudinally and pinned flat. Plaque area per total intimal area was determined using image

analysis software (ImageJ, NIH).

2.11. Toxicity serum biomarker evaluation

Plasma levels of LDL-cholesterol (LDL-c), HDL-cholesterol (HDL-c), total cholesterol (TC) and triglycerides (TG) were analyzed by the Clinical Chemistry Laboratory of the Michigan Diabetes Research and Training Center. Aspartate aminotransferase (AST) and alanine aminotransferase (ALT) were determined using kits from Sigma.

2.12. Statistical analysis

Statistical comparisons and analyses were performed by two-tailed unpaired Student's *t*-test. A p value < 0.05 was considered statistically significant. Data are presented as mean ± S.E.M.

3. Results

3.1. The impact of peptide to lipid ratio on sHDL size and purity

In order to encapsulate hydrophobic T1317, it was dissolved in a mixture of organic solvents with 22A peptide and phospholipids and subsequently lyophilized to form a homogeneous solid mixture of three components. Similar procedures were used by us to prepare sHDL-incorporated chemotherapeutics agents [31,33]. The lyophilized mixture was subsequently hydrated with PBS and thermally cycled to facilitate peptide-lipid binding and sHDL nanoparticle assembly. The impact of lipid to peptide ratio on nanoparticle average particle size, purity and drug loading efficiency was examined for 22A-DMPC/POPC nanoparticles prepared at 1:1, 1:2 and 1:4 (w/w) peptide to phospholipid ratio at the theoretical T1317 loading of 2.5% (w/w). When the peptide to phospholipid ratio was increased from 1:1 to 1:4, the average size of sHDL-T1317 nanoparticles increased from 9.82 ± 0.18 to 19.53 ± 0.26 nm (Table S1) and drug encapsulation efficiency increased from 69.5 ± 2.0 to 96.8 ± 0.3% (Fig. 1a). However, the sHDL-T1317 prepared at 1:4 w/w ratio contained liposomal impurities, likely due to an insufficient amount of peptide to wrap around the lipid bilayers (see Supplementary data, Fig. S1a). The increase in particle size and decrease in sHDL purity at a higher lipid to peptide ratio was consistent with our previous reports [34]. In addition, clinically tested 22A-based sHDL, ETC-642, had an approximate 1:2 w/w peptide to lipid ratio [35,36]. Based on these factors, a 1:2 w/w ratio was selected for further testing.

3.2. Optimization of sHDL composition for effective drug loading

Due to its hydrophobic nature, T1317 partitions in the phospholipid membrane of sHDL and drug encapsulation efficiency depends on the physicochemical properties of the phospholipid selected to prepare nanoparticle. Several types of phospholipids varying in fatty acid chain length, degree of saturation, as well as transition temperature were used to prepare sHDL. T1317 was loaded at the theoretical loadings of 1.25, 2.50 and 5.00% weight of drug per weight of particle. The unencapsulated drug was removed by desalting column and T1317 remaining in sHDL was determined by HPLC (Fig. 1a). The purity of resulting sHDL particles was analyzed by gel permeation chromatography (GPC) (Fig. 1b). When sHDL was prepared using saturated phospholipids with gel transition temperatures (T_g) above 37 °C, the loading efficiency of T1317 was around 40–55%, as drug affinity for "rigid" lipid bilayers was

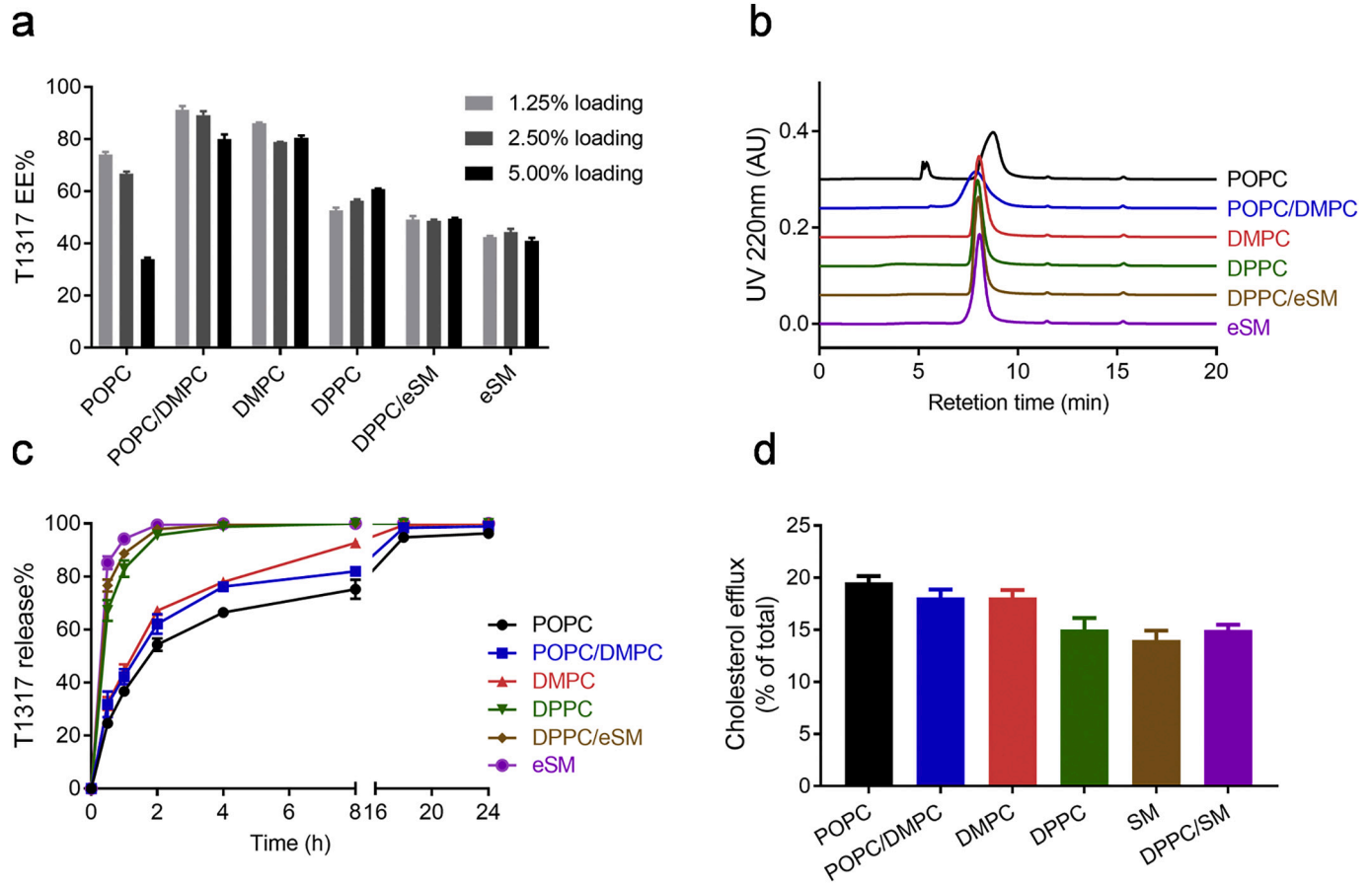

Fig. 1. Preparation and characterization of different T1317-sHDL nanoparticles. The effect of sHDL lipid composition on T1317 encapsulation efficiency for 1.25, 2.5 and 5% drug loading (a); the effect of lipid composition on sHDL purity for 2.5% drug loading (b); *in-vitro* accelerated T1317 release for sHDL with 2.5% drug loading (c); cumulative 8 h cholesterol efflux from J774.1 macrophages by blank sHDL with different lipid compositions (d).

low. All but one sHDL preparations formed pure and homogeneous sHDL particles with GPC retention time of ~8 min. When POPC, a very low T_g (−2 °C) phospholipid, was used to prepare sHDL-T1317 nanoparticles, the particle GPC purity was low due to the presence of liposomal impurities on the chromatogram with retention time of ~5 min. However, the use of DMPC or DMPC-POPC mixtures resulted in pure and homogeneous sHDL-T1317 nanoparticles with an encapsulation efficiency above 75%.

3.3. The impact of sHDL lipid composition on drug release

Due to the low aqueous solubility of T1317 in PBS, the *in vitro* release study was conducted in the presence BioBeads™ SM-2, a strong adsorbent of hydrophobic substances. BioBeads™ were added to the release media to rapidly bind to the released T1317, create sink conditions and facilitate additional drug release. BioBeads™ are capable of completely adsorbing T1317 in the 50 μg/mL solution within 10 min incubation (data not shown). Based of release data, LXR agonist appeared to have a lower affinity to "rigid" bilayers of sphingomyelin and DPPC, resulting in rapid drug release for these sHDL compositions. In contrast, the sHDL composed of lipids with $T_g < 37$ °C (DMPC, POPC and DMPC/POPC mixture) were able to retain T1317 longer (Fig. 1c).

3.4. The effect of sHDL composition on cholesterol efflux capacity

To examine the effect of sHDL phospholipid composition on its ability to efflux cholesterol, J774.1 murine macrophages were loaded with ^{3}H-labeled cholesterol and subsequently incubated with sHDL of various compositions. As expected all sHDL nanoparticles effluxed cholesterol from macrophages (Fig. 1d). During 8 h of incubation with blank sHDL, efflux was slightly higher for sHDL prepared with POPC, DMPC and POPC/DMPC mixtures, likely because the T_g of these lipid bilayers is below 37 °C and cholesterol freely partitions in these sHDL. Based on *in vitro* evaluation, DMPC-sHDL and POPC/DMPC-sHDL particles, which have higher T1317 encapsulation efficiency, higher sHDL nanoparticle purity, slower release in accelerated conditions and higher cholesterol efflux capacity, were selected to examine their ability to increase ABCA1/ABCG1 expression in macrophages *in vitro*.

3.5. Effect of T1317-sHDL on ABCA1/ABCG1 expression and subsequent cholesterol efflux from macrophages

Next, we compared the abilities of the two selected formulations, DMPC-sHDL and POPC/DMPC-sHDL nanoparticles containing T1317, to upregulate expression of ABCA1 and ABCG1 and facilitate cholesterol efflux. ABCA1 and ABCG1 transporters mediated cellular cholesterol efflux from cholesterol loaded macrophages (foam cells) to extracellular acceptors such as apoA-I and HDL particles. Transcription of ABCA1 and ABCG1 was highly induced upon cholesterol loading and activation of the nuclear receptors LXR. Both of DMPC/sHDL-T1317 and POPC/DMPC/sHDL-T1317 nanoparticles upregulated the gene expression of ABCA1 and ABCG1 after 4 h incubation, which was slightly higher for the sHDL loaded-drug compared to free T1317-treatment (Fig. 2a-b). The treatment of macrophages with POPC/DMPC/sHDL-T1317 showed the greatest increase in ABCA1 expression relative to DMPC/sHDL-T1317 ($p < 0.05$) and free T1317 treatments ($p < 0.01$).

Next, the protein level of ABCA1 was detected by Western Blotting after 24 h incubation. Similar to gene expression, both DMPC/sHDL-T1317 and POPC/DMPC/sHDL-T1317 nanoparticles increased ABCA1 protein levels in a dose-dependent manner similar to free drug (Fig. 2c), indicating that sHDL delivered T1317 compound into the macrophage and activated the LXR pathway. Finally, we examined if sHDL-mediated delivery of T1317 to macrophages could increase functional cholesterol efflux to endogenous cholesterol acceptors, apoA-I and HDL. ABCA1-mediated cholesterol efflux is known to occur primarily to the lipid-poor or lipid-free apoA-I. Consistent with increased gene expression results, the ABCA1-mediated cholesterol efflux (apoA-I as acceptor) was higher for POPC/DMPC-sHDL-T1317 relative to DMPC-sHDL-T1317 and free T1317 (Fig. 2d-e). Based on the characterization of sHDL-T1317 purity, drug encapsulation efficiency, drug release and ability to upregulate ABCA1/ABCG1 expression and facilitate cholesterol efflux, the POPC/DMPC-based sHDL-T1317 nanoparticles were selected for evaluation *in vivo*.

3.6. Characterization of size and serum stability of optimized T1317-sHDL prior to in vivo studies

The optimized POPC/DMPC-based sHDL nanoparticles, both blank or containing either DiD dye or T1317, were prepared for *in vivo* testing and characterized. The average volume particle size of T1317-sHDL was determined to be 10.5 ± 0.1 nm by DLS (Fig. 3a). When blank and drug loaded sHDL were analyzed by transmission electron microscopy similar nanoparticle morphology and particle size were observed (Fig. 3b). Despite the low transition temperature of lipids, sHDL particles presented good particle stability during incubation under 4 °C, 25 °C and 37 °C (Fig. S2).

Similar to endogeneous HDLs, following administration *in vivo,* sHDL nanoparticles are known to interact with endogenous lipoproteins by exchanging lipid, protein and cargo components in a process of lipoprotein remodeling [37–39]. The beneficial interaction between endogenous HDL and sHDL is known to occur in patients and animal models following sHDL infusion leading to increase levels of endogenous lipid-poor HDL and enhanced ABCA1 mediated cholesterol efflux and atheroma reduction [37,40]. Endogenous lipoproteins have been found to adsorb to the surface of nanoparticles forming a protein corona, facilitating their remodeling and drug release [41–44]. To assess the remodeling of T1317-sHDL by endogenous lipoproteins, nanoparticles were incubated with freshly pooled serum from C57BL/6 mice, and the serum lipoproteins were then separated by size exclusion chromatography (SEC). The T1317 distribution between lipoprotein fractions was detected by monitoring the T1317 concentration in elution fractions after SEC. The T1317-sHDL particles appeared to be slightly larger than endogenous sHDL with a SEC retention time difference of ~1 min. Initially after mixing with serum, T1317 retained in the sHDL fraction, however after 8 h of incubation, the T1317 eluted together with endogenous HDL (Fig. 3c-d).

Although T1317 appeared to exchange between sHDL and endogenous HDL, it was preferentially retained in the HDL fraction and showed little movement to LDL and VLDL lipoproteins. Thus, it is likely that *in vivo,* T1317 will be delivered to the atheroma by sHDL and endogenous HDL particles, leading to LXR activation and facilitation of cholesterol efflux.

3.7. Synthetic HDL nanoparticles deliver cargo to macrophages in vitro and in vivo

Next, we examined the ability of sHDL to deliver its cargo to macrophages *in vitro*. Fluorescently labeled sHDL was incubated with human THP-1 monocytes differentiated macrophages. Non-labeled sHDL was used as a negative control. DiD fluorescence in the cells could be detected after 30 min of incubation, with the intensity of the signal increasing over time (Fig. 4a-b). After 2 h incubation, 99% of cells were DiD positive, indicating that sHDL successfully delivered its cargo to the macrophages.

To evaluate the ability of sHDL to deliver its cargo to atherosclerotic plaques, ApoE-deficient mice were placed on HFHC diet for 12 weeks to induce atherosclerotic plaque formation. The animals were injected intraperitoneally with sHDL-DiD, and accumulation of fluorescent DiD in the aorta was confirmed 4 h after injection [29]. To examine if sHDL-DiD was delivered specifically to atheroma macrophages, obtained tissue sections were stained with an anti-CD-68 antibody, specific for monocytes and macrophages. As illustrated in Fig. 4c, DiD signal co-

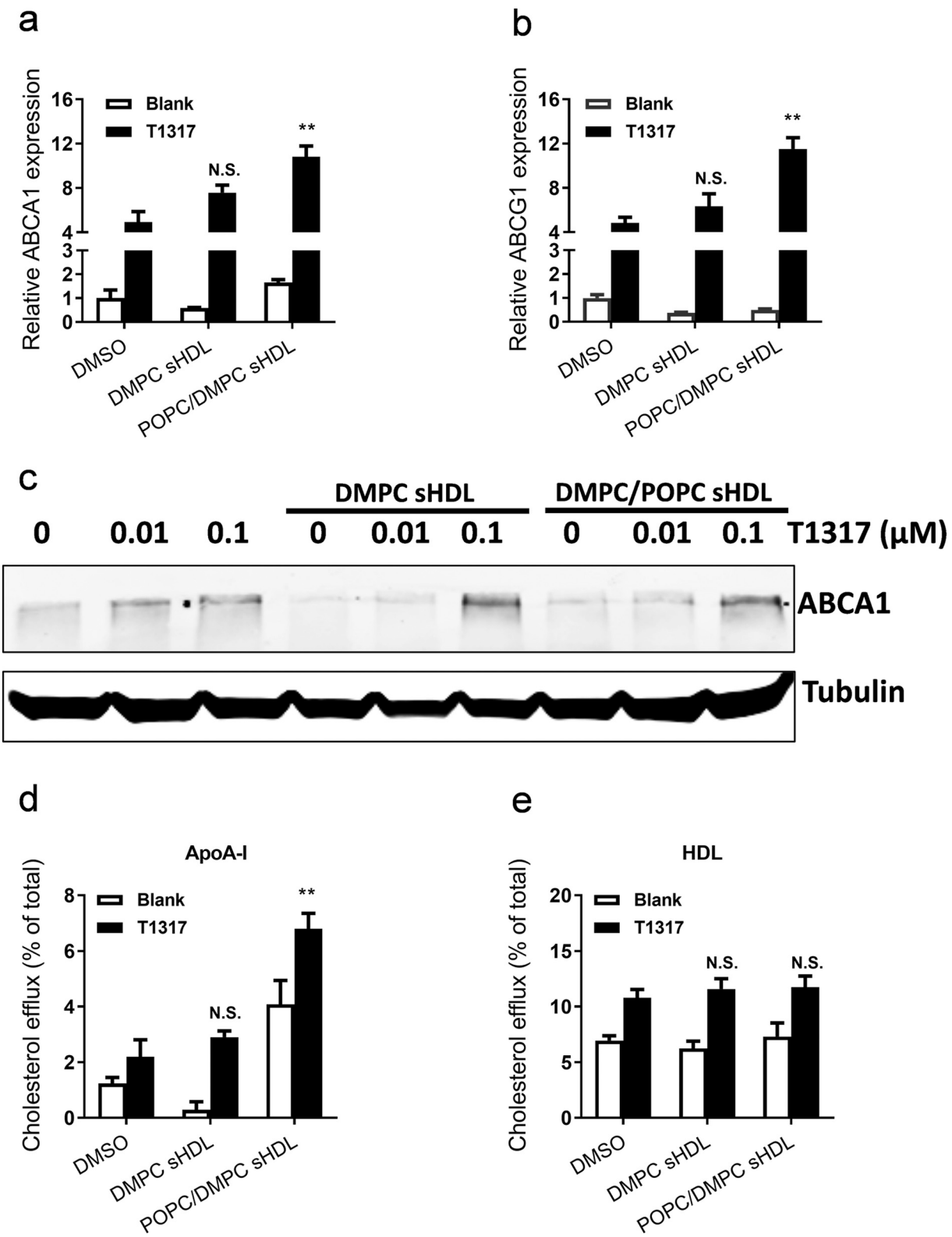

Fig. 2. Effect of different T1317-HDLs on ABCA1/ABCG1 expression and cholesterol efflux *in vitro*. Levels of ABCA1 and ABCG1 mRNA in J774 cells (a-b) induced by DMPC-HDL or POPC/DMPC-HDL (10 μg/mL 22A) without T1317 (white column) or with T1317 (black column) after 4 h treatment. The expression of ABCA1 was verified by Western blotting after 24 h treatment with different sHDL (10 μg/mL 22A) (c). Cholesterol efflux induced by overnight incubation with indicated formulations followed by incubation with apoA-I as the acceptor (d) or commercial human HDL as the acceptor (e). (**$P < 0.01$, N.S. no significant difference, *versus* DMSO-T1317 (free T1317) group).

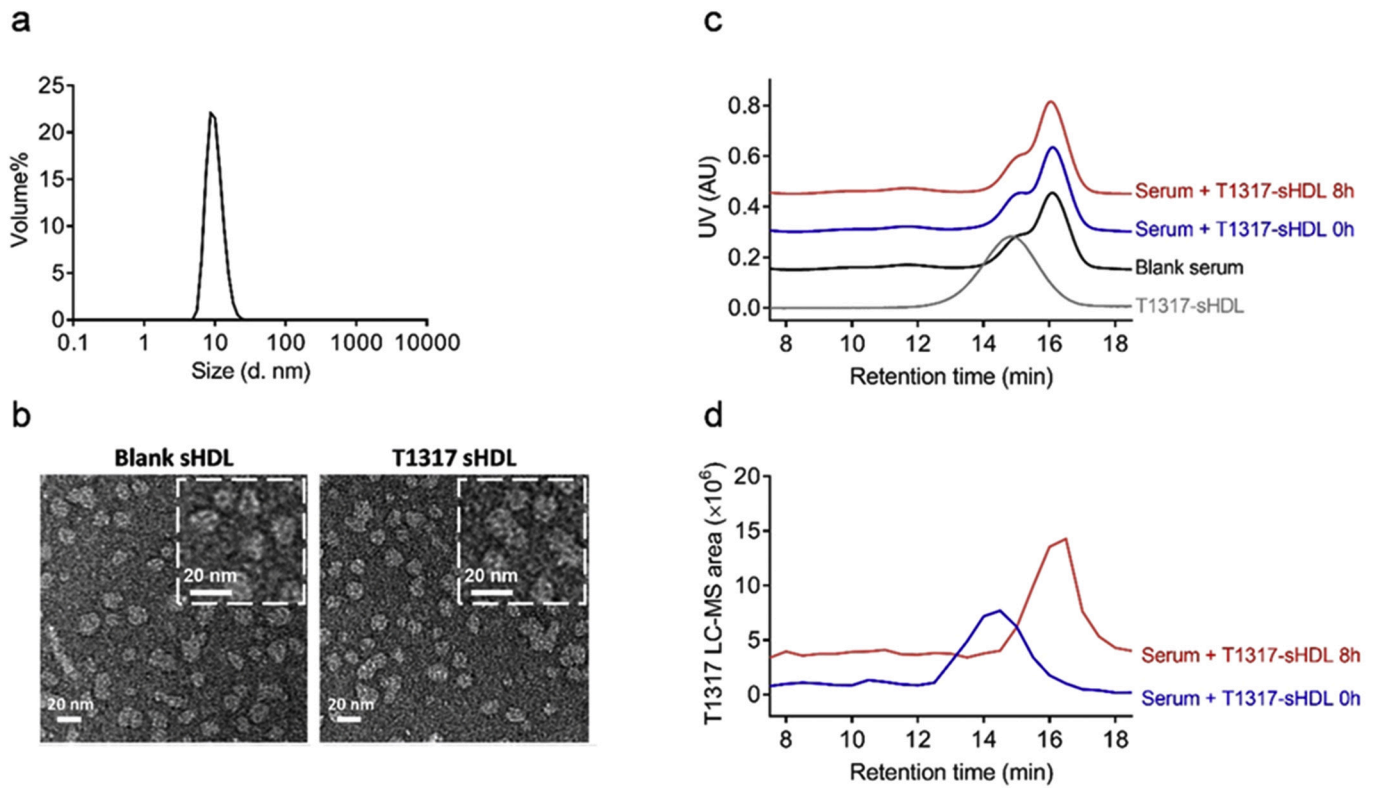

Fig. 3. *In vitro* characterization of optimized T1317-sHDL (T1317-POPC/DMPC-sHDL). Size distribution of T1317-sHDL (a); TEM pictures of the optimized blank sHDL and T1317-sHDL, scale bar was 20 nm (b). Remodeling of optimized LXR-HDLs in C57 mouse serum (c-d). T1317-sHDL were incubated with fresh serum from normal C57 mice at 0 and 8 h. Incubation mixture was then analyzed by HPLC equipped with a Sepharose column at 220 nm and 260 nm to locate the different lipoprotein and sHDL (c), and the concentration of T1317 in all elution fractions was quantified *via* UPLC-MS (d).

localized with CD68-positive cells in the atherosclerotic plaques. From these findings, we can conclude that sHDL is not only capable of accumulating in atheroma area following *in vivo* dosing, but also capable of delivering its cargo to macrophages efficiently.

3.8. Synthetic T1317-HDL nanoparticles inhibited atherosclerosis development in vivo

Thus far, we have shown that sHDL nanoparticles are capable of delivering cargo to the atheroma *in vivo*. More specifically, these sHDLs can be loaded with and deliver the LXR agonist, T1317, to atheroma macrophages. Not only does this result in increased ABCA1 expression *via* T1317, but sHDL itself can also serve as an acceptor of the effluxed cholesterol. To examine whether this multifaceted drug delivery system could achieve a greater therapeutic effect over free drug or sHDL alone, we tested our nanoparticles in an ApoE-deficient murine model of atherosclerosis. Because we expected to see a synergy between sHDL delivery and cholesterol acceptor capacity, we chose a relatively low dose of T1317 (1.5 mg/kg) and sHDL (30 mg/kg) for the therapeutic study. In contrast, T1317 doses as high as 10–50 mg/kg have been previously used to achieve therapeutic effect in animals studies [10,15,46] and sHDL clinical doses have reached up to 135 mg/kg [45].

ApoE-deficient mice were placed on a HFHC diet for 6 weeks, then randomly divided into 5 groups, receiving IP injections three times per week with: (i) DMSO vehicle control (DMSO), (ii) T1317 compound at 1.5 mg/kg in DMSO (T1317), (iii) PBS control (PBS), (iv) sHDL at 30 mg/kg 22A in PBS (sHDL), and (v) T1317-sHDL in PBS (30 mg/kg 22A containing 1.5 mg/kg T1317). At the end of the 6-week treatment, animals were sacrificed and whole aortas excised for plaque area analysis by oil red O staining (Fig. 5a-b). Both control groups (DMSO and PBS) showed similar en face aortic plaque area (17.1 ± 2.1% *vs* 18.7 ± 3.7%). T1317 treatment halted progression of atheroma development with an average aortic plaque area of 12.2 ± 2.0% (28% lower as compared to DMSO control). As expected, treatment with sHDL itself halted progression of atheroma development with an average aortic plaque area of 10.8 ± 1.3% (42% lower as compared to PBS control). Most importantly, sHDL-T1317 treatment showed a remarkable reduction in atherogenesis with aortic plaque area of 4.9 ± 1.1% (73% lower than plaque area of PBS control). The efficacy of sHDL-T1317 was superior to the efficacy of either sHDL or T1317 alone, indicating a synergic effect between the atheroma delivery of T1317 and cholesterol acceptor capacity of sHDL.

3.9. Reduced LXR-agonist induced liver toxicity due to low dose and sHDL delivery

Systemic administration of LXR agonists is known to upregulate lipogenesis genes in the liver, leading to increased sterol and fatty acid synthesis and subsequent elevation in plasma cholesterol and triglyceride levels. These side effects were observed in animal and clinical studies for several LXR ligands, leading to the discontinuation of their clinical development. To examine whether these side effects would still occur following low-dose (1.5 mg/kg), nanoparticle mediated T1317 administration, plasma levels of cholesterol, triglycerides and enzymes correlating with reduced liver function, ALT/AST, were determined at the terminus of the therapeutic study. Lipid profiling results showed no difference in total cholesterol, HDL-C and LDL-C levels between groups (Fig. 6a-c). Treatment with T1317 alone increased triglyceride levels compared to PBS and sHDL groups, but T1317-sHDL did not have this effect (Fig. 6d). Six-week treatment did not trigger liver damage, as no significant changes in ALT and AST levels were observed (Fig. 6e,f). Taken together, the low dose of T1317 required to produce a therapeutic response due to the dual atheroma targeting and cholesterol acceptor effects of T1317-sHDL resulted in fewer side effects, and sHDL incorporation of T1317 further improved its safety.

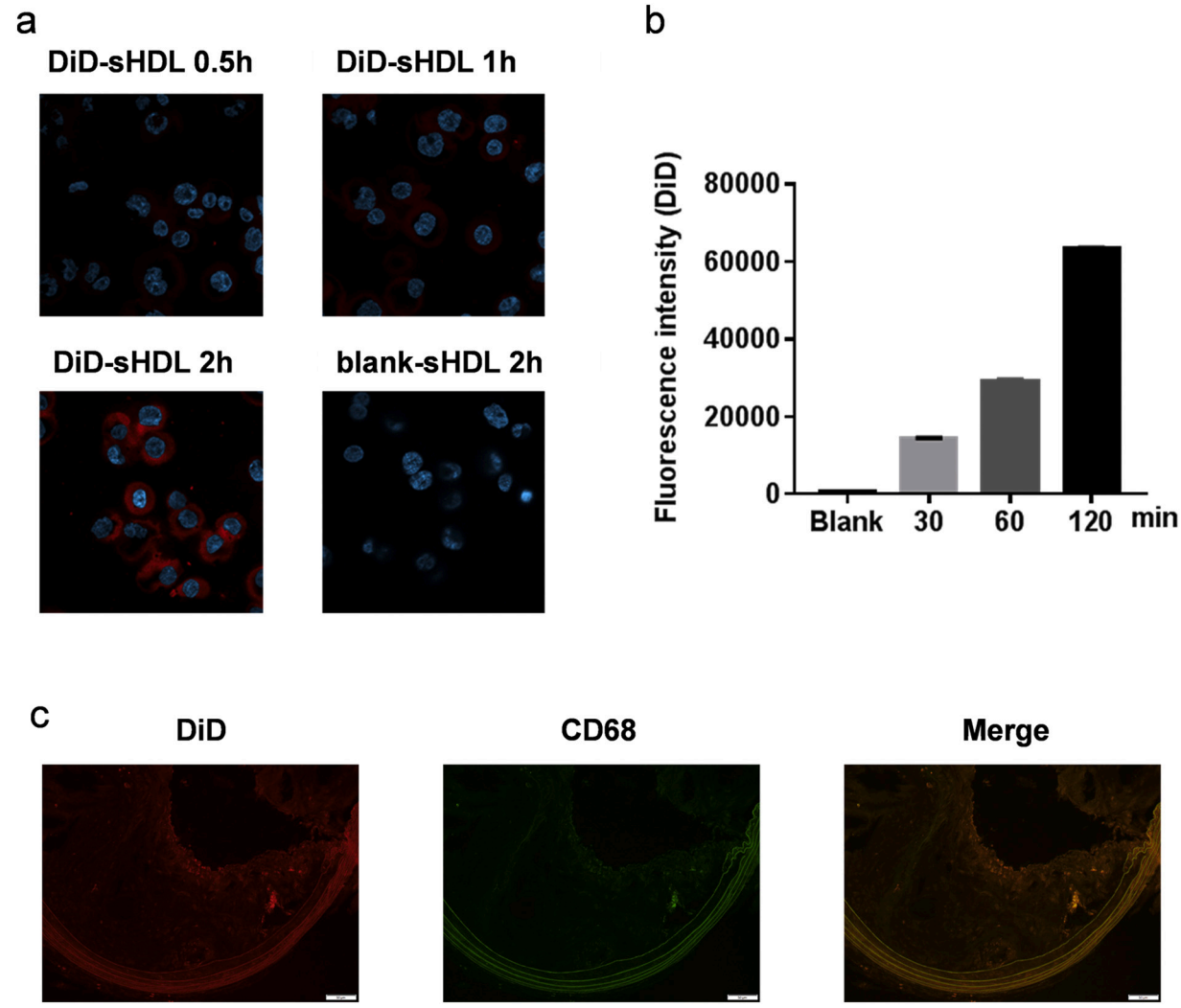

Fig. 4. *In vitro* and *in vivo* macrophage uptake with blank POPC/DMPC sHDL and DiD-POPC/DMPC sHDL. Cellular uptake of indicated formulations by human THP-1 monocytes differentiated macrophages analyzed with confocal microscopy (a) and flow cytometry (b). Immunofluorescence of sections from the plaque showing DiD-loaded sHDL accumulated in CD68+ macrophages.

4. Discussion

In the current study, we describe how the composition of T1317-sHDL nanoparticles was optimized to maximize LXR agonist encapsulation efficiency, drug retention, nanoparticle purity, upregulation of ABCA1/ABCG1 gene expression, and facilitation of cholesterol efflux from macrophages. The selected T1317-sHDL nanoparticles accumulated in atheroma macrophages in ApoE$^{-/-}$ mice on a HFHC diet. Most importantly, T1317-sHDL nanoparticles showed a greater inhibition of aortic plaque formation, with an average atheroma area of 4.9% relative to 12.2% and 10.8% following treatment with T1317 or sHDL alone, respectively. Previously, we used T1317-sHDL nanoparticles to treat atherosclerosis in a severe atherosclerosis regression study, in which ApoE$^{-/-}$ mice were fed a HFHC diet for 14 weeks to induce atherosclerotic plaque formation, and then the mice were placed to normal chow diet at the same time as the start of treatment [29]. In that study, we show significant plaque regression for animals treated with T1317-sHDL (15.0%, $p < 0.05$) compared to 24.1% for control animals treated with PBS. However, due to the severity of atherosclerotic plaque formation in animals, no statistically significant plaque regression was observed after treatment with low dosage of T1317 or sHDL alone, with average atheroma areas of 21.6% and 20.6%, respectively [29]. In the current study, we were able to confirm that both free T1317 and sHDL could slow the progression of atherogenesis, but the combined atheroma delivery and cholesterol acceptor modality of T1317-sHDL produced superior efficacy. Together these two studies show the ability of T1317-sHDL to regress severe atherosclerosis and to halt further progression of atherogenesis.

In order to optimize T1317-sHDL nanoparticle purity and size, we first altered the lipid to peptide ratio used in sHDL formation. We found that sHDL prepared at 2:1 lipid to peptide weight ratio had an optimal size of 10.5 ± 0.1 nm and sHDL particle purity exceeding 97%. Then, we explored how the type of phospholipid used to prepare sHDL impacts drug encapsulation efficiency (EE%) and *in vitro* release. When sHDL were prepared with rigid phospholipids ($T_g > 37$ °C) like SM, DPPC and SM/DPPC mixtures, T1317 released rapidly and EE was low. In opposite, longer drug retention and higher EE (> 80%) were observed for T1317-sHDL prepared with phospholipids with $T_g < 37$ °C, such as POPC, DMPC and POPC/DMPC mixture. However, the purity of POPC-based sHDL was poor, as the very low T_g of POPC (−2 °C) appears to affect the stability of sHDL particles and leads to the formation of liposomal impurities. We also examined how phospholipid composition impacts the cholesterol acceptor capacity of blank sHDL nanoparticles, showing that POPC, DMPC and POPC/DMPC-based blank sHDL are superior cholesterol acceptors. Finally, we determined the abilities of drug loaded DMPC and DMPC/POPC-sHDL to upregulate ABCA1 and ABCG1

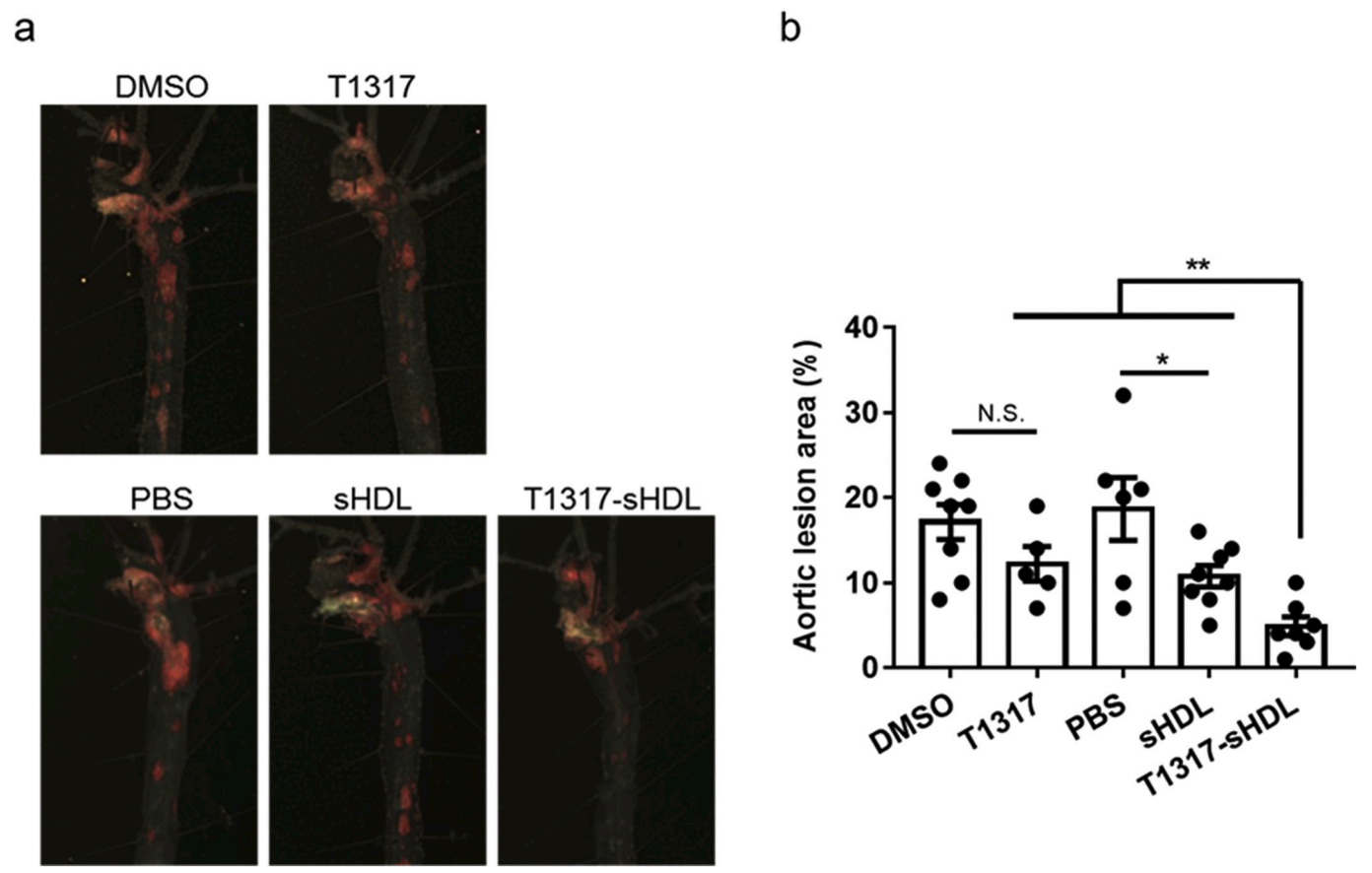

Fig. 5. Effect of T1317-sHDL on atherosclerosis development in ApoE$^{-/-}$ mice. Aortas were dissected and plaque areas visualized by oil red O staining. Representative lesion images (a) and corresponding quantitative analyses of whole aorta trees (b). n = 5–8 animals per group, * $p < 0.05$, ** $p < 0.01$ and N.S. no significant difference.

expression and facilitate cholesterol efflux from macrophages. Based on the results of these cell culture experiments, DMPC/POPC T1317-sHDL were selected for *in vivo* evaluation due to their superior *in vitro* efficacy.

The advantages of our approach include utilization of the dual aspect of sHDL, first, to deliver LXR agonist T1317 to the atheroma and, second, to serve as cholesterol acceptor in circulation. Due to this multifaceted therapeutic mechanism, the antiatherogenic efficacy of T1317-sHDL nanoparticles was observed at T1317 doses significantly lower than those previously used in atherosclerosis models. Both severe atherosclerosis and atherogenesis models were dosed by T1317-sHDL at 1.5 mg T1317/kg 3 times a week by intraperitoneal administration (4.5 mg/kg/week dose). In contrast, T1317 doses as high as 10 mg/kg daily oral gavage (70 mg/kg/week) [46] and 50 mg/kg daily intravenous dosing (350 mg/kg/week) [15] were needed to show pharmacological efficacy in animal models of atherosclerosis. Due to the drastic reduction in T1317 dose used in our study, many liver side effects triggered by LXR agonist treatment were avoided (Fig. 6). Some increase in plasma and hepatic triglyceride levels and upregulation of hepatic lipogenesis genes (Srebp1c, Fasn and Scd1) were observed for free T1317 group, but incorporation of T1317 in sHDL nanoparticles abolished these side effects [29].

Several other nanoparticle approaches have been used to deliver LXR agonists to the atheroma [17,19,47,48]. One such approach utilizes nanoparticles made from PLGA-b-PEG polymer alone (NP-LXR, ~140 nm diameter), or mixture of the polymer and phosphatidylserine (PSNP-LXR, ~160 nm diameter), to deliver the LXR agonist, GW3965 [19,47,48]. When these nanoparticles were tested in an *Ldlr*$^{-/-}$ mouse model of atherosclerosis fed a high fat diet for 16 weeks, six retro-orbital doses of NP-LXR at 10 mg/kg resulted in a 50% reduction in plaque macrophage content [48]. This reduction was greater relative to the same doses free GW3956. Moreover, incorporation of GW3965 in nanoparticles reduced liver lipogenesis gene upregulation relative to free drug [19]. Another approach utilized HDL-like nanoparticles prepared from full-length apoA-I protein, phospholipids and polymers for GW3965 delivery [17]. The size of these HDL-like particles, ~30 nm in diameter, appears to be slightly larger than the size of endogenous HDL (~10–14 nm). Following IV administration in *ApoE*$^{-/-}$ atherosclerotic mice, drug-loaded HDL particles accumulated in aortic plaque and exhibited local anti-inflammatory effect, however, direct advantage of HDL-GW3965 in treatment of atherosclerosis relative to free drug or blank HDL has not been shown. ApoA-I is a large protein (human apoA-I has 243 amino acid residues), making it difficult and expensive to synthesize high quality HDL particles for venous administration. The use of synthetic peptides for drug delivery has potentially multiple advantages over the use of fulllength apoA-I.

Variations in experimental conditions used to evaluate pharmacological effects LXR-nanoparticles makes it difficult to directly compare the efficacy of different types of LXR atheroma drug delivery systems. The genotype of murine model of atherosclerosis (ApoE$^{-/-}$ or Ldlr$^{-/-}$), duration of high fat diet, type of LXR agonists used, treatment regimen (route of administration, dose, dosing frequency and duration) vary significantly among those published reports on nanoparticle based LXR delivery. Here using the sHDL nanoparticles, we are the first to show a synergy in anti-atherosclerosis effect between atheroma targeting of LXR ligand and cholesterol acceptor capacity of the nanocarrier itself. The sHDL used in the current study has been shown to facilitate cholesterol efflux in animals and dyslipidemic patients [26,30,35]. Because these sHDL nanoparticles have been already tested in patients,

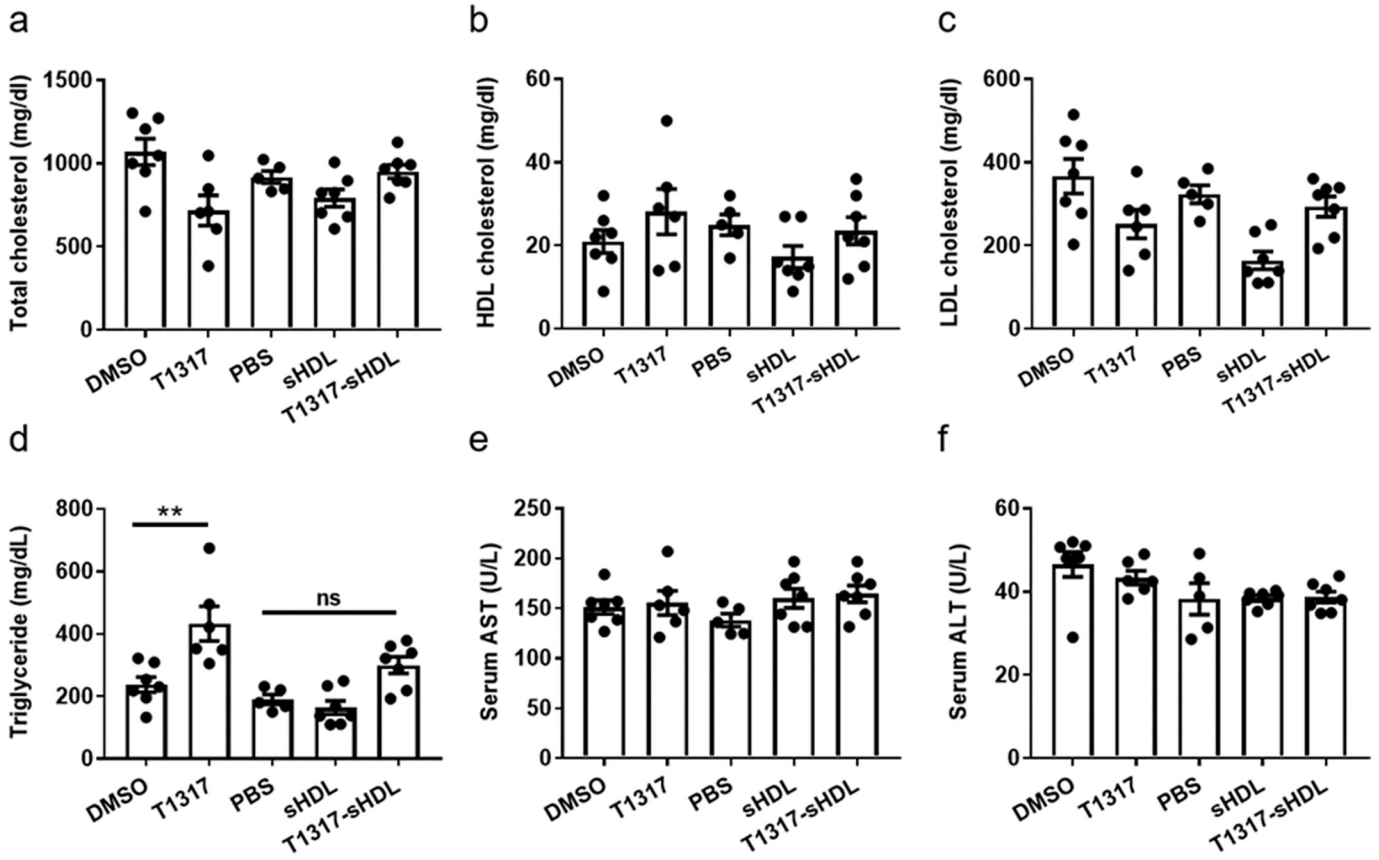

Fig. 6. Treatment with T1317-sHDL decreased the side effect of Free T1317. After treatment with different formulation for 6 weeks, plasma total cholesterol (a), HDL cholesterol (b), LDL cholesterol (c), triglycerides (d), aspartate aminotransferase (AST) (e) and alanine aminotransferase (ALT) (f) were measured. $n = 5–9$ per group; $^{**}P < 0.01$ compared to controls.

their manufacturing under current good manufacturing practices (cGMP) is established and these processes could be easily adapted to incorporate LXR ligands. In addition, completed toxicology evaluations, filed investigational drug applications with US FDA and proven clinical safety for sHDL as a cholesterol acceptor will likely facilitate its clinical translation as a nanocarrier.

LXR agonists belong to a very interesting class of compounds. Apart from their efficacy in regulating cholesterol efflux in atheroma macrophages leading to reduction of atherosclerosis in animal models, their utility has been explored in treatment of retinal diseases, Alzheimer's disease, diabetes and dermatitis [2,4,49,50]. Several products have reached clinical development, including LXR-623 (Wyeth) [51], CS-8080 (Daiichi Sankyo) [52], BMS-779788 and BMS-852927 (Exelixis/BMS) [53,54]. Unfortunately, clinical development of many LXR agonists has been discontinued due to hepatic or neuropsychiatric side effects in early clinical trials. Thus, targeted nanoparticle based approaches would be very beneficial for the selective delivery of LXR agonists to atheroma [17,29], brain or eye, all while reducing liver accumulation. With this in mind, the efficacy at lower doses observed by us along with reduced toxicity due to nanoparticle administration seen by us and several other investigators could spark a renewed interest to the entire class of LXR agonists.

Acknowledgements

This study was supported by NIH grants HL068878 and HL134569 (to Y.E.C.), GM113832 and NS091555 (to A.S.), HL134569 (to Y.E.C. and A.S.), American Heart Association grants 15SDG24470155 (to Y.G.), 13SDG17230049 (to A.S.), AHA 16POST27760002 (to W.Y.), 15PRE25090050 (to R.K), 19PRE34400017 (to M.Y.), T32 GM008353 (EM) and T32-HL125242 (EM).

Appendix A. Supplementary data

Supplementary data to this article can be found online at https://doi.org/10.1016/j.jconrel.2020.11.016.

References

[1] M.V. Cannon, et al., LXRα improves myocardial glucose tolerance and reduces cardiac hypertrophy in a mouse model of obesity-induced type 2 diabetes, Diabetologia 59 (3) (2016) 634–643.
[2] G. Cao, et al., Antidiabetic action of a liver x receptor agonist mediated by inhibition of hepatic gluconeogenesis, J. Biol. Chem. 278 (2) (2003) 1131–1136.
[3] Z. Ma, et al., Liver X receptors and their agonists: targeting for cholesterol homeostasis and cardiovascular diseases, Curr. Issues Mol. Biol. 22 (2017) 41–64.
[4] R.K. Sodhi, N. Singh, Liver X receptors: emerging therapeutic targets for Alzheimer's disease, Pharmacol. Res. 72 (2013) 45–51.
[5] I.L. Aye, et al., Placental ABCA1 and ABCG1 transporters efflux cholesterol and protect trophoblasts from oxysterol induced toxicity, Biochim. Biophys. Acta 1801 (9) (2010) 1013–1024.
[6] P. Costet, et al., Sterol-dependent transactivation of theABC1 promoter by the liver X receptor/retinoid X receptor, J. Biol. Chem. 275 (36) (2000) 28240–28245.
[7] B.A. Kingwell, et al., HDL-targeted therapies: progress, failures and future, Nat. Rev. Drug Discov. 13 (6) (2014) 445.
[8] S.B. Joseph, et al., Synthetic LXR ligand inhibits the development of atherosclerosis in mice, Proc. Natl. Acad. Sci. 99 (11) (2002) 7604–7609.
[9] A. Kratzer, et al., Synthetic LXR agonist attenuates plaque formation in apoE−/−mice without inducing liver steatosis and hypertriglyceridemia, J. Lipid Res. 50 (2) (2009) 312–326.
[10] L. Verschuren, et al., LXR agonist suppresses atherosclerotic lesion growth and promotes lesion regression in apoE* 3Leiden mice: time course and mechanisms, J. Lipid Res. 50 (2) (2009) 301–311.
[11] A. Grefhorst, et al., Stimulation of lipogenesis by pharmacological activation of the liver X receptor leads to production of large, triglyceride-rich very low density lipoprotein particles, J. Biol. Chem. 277 (37) (2002) 34182–34190.

[12] P.H. Groot, et al., Synthetic LXR agonists increase LDL in CETP species, J. Lipid Res. 46 (10) (2005) 2182–2191.
[13] J.R. Schultz, et al., Role of LXRs in control of lipogenesis, Genes Dev. 14 (22) (2000) 2831–2838.
[14] T. Yoshikawa, et al., Identification of liver X receptor-retinoid X receptor as an activator of the sterol regulatory element-binding protein 1c gene promoter, Mol. Cell. Biol. 21 (9) (2001) 2991–3000.
[15] J.E. Feig, et al., LXR promotes the maximal egress of monocyte-derived cells from mouse aortic plaques during atherosclerosis regression, J. Clin. Invest. 120 (12) (2010).
[16] E.M. Quinet, et al., Gene-selective modulation by a synthetic oxysterol ligand of the liver X receptor, J. Lipid Res. 45 (10) (2004) 1929–1942.
[17] J. Tang, et al., Immune cell screening of a nanoparticle library improves atherosclerosis therapy, Proc. Natl. Acad. Sci. 113 (44) (2016) E6731–E6740.
[18] N. Terasaka, et al., T-0901317, a synthetic liver X receptor ligand, inhibits development of atherosclerosis in LDL receptor-deficient mice, FEBS Lett. 536 (1–3) (2003) 6–11.
[19] M. Yu, et al., Targeted nanotherapeutics encapsulating liver x receptor agonist gw3965 enhance antiatherogenic effects without adverse effects on hepatic lipid metabolism in Ldlr−/− mice, Adv. Healthc. Mater. 6 (20) (2017) 1700313.
[20] R. Duivenvoorden, et al., A statin-loaded reconstituted high-density lipoprotein nanoparticle inhibits atherosclerotic plaque inflammation, Nat. Commun. 5 (2014) 3065.
[21] A. Iwata, et al., Antiatherogenic effects of newly developed apolipoprotein AI mimetic peptide/phospholipid complexes against aortic plaque burden in Watanabe-heritable hyperlipidemic rabbits, Atherosclerosis 218 (2) (2011) 300–307.
[22] C.J. Fielding, P.E. Fielding, Molecular physiology of reverse cholesterol transport, J. Lipid Res. 36 (2) (1995) 211–228.
[23] R. Easton, et al., A multiple ascending dose study of CSL112, an infused formulation of ApoA-I, J. Clin. Pharmacol. 54 (3) (2014) 301–310.
[24] G.K. Hovingh, et al., The effect of an apolipoprotein AI–containing high-density lipoprotein–mimetic particle (CER-001) on carotid artery wall thickness in patients with homozygous familial hypercholesterolemia: the Modifying Orphan Disease Evaluation (MODE) study, Am. Heart J. 169 (5) (2015) 736–742 (e1).
[25] S.E. Nissen, et al., Effect of recombinant ApoA-I Milano on coronary atherosclerosis in patients with acute coronary syndromes: a randomized controlled trial, JAMA 290 (17) (2003) 2292–2300.
[26] J. Miles, et al., P105 single-dose tolerability, pharmacokinetics, and cholesterol mobilization in Hdl-c fraction following intravenous administration of Etc-642, a 22-mer Apoa-i analogue and phospholipids complex, in atherosclerosis patients, Arterioscler. Thromb. Vasc. Biol. 24 (5) (2004) e19.
[27] J.-C. Tardif, et al., Effects of the high-density lipoprotein mimetic agent CER-001 on coronary atherosclerosis in patients with acute coronary syndromes: a randomized trial, Eur. Heart J. 35 (46) (2014) 3277–3286.
[28] J.-C. Tardif, et al., Effects of reconstituted high-density lipoprotein infusions on coronary atherosclerosis: a randomized controlled trial, Jama 297 (15) (2007) 1675–1682.
[29] Y. Guo, et al., Synthetic high-density lipoprotein-mediated targeted delivery of liver X receptors agonist promotes atherosclerosis regression, EBioMedicine 28 (2018) 225–233.
[30] Dasseux, J.-L., A.S. Schwendeman, and L. Zhu, Apolipoprotein AI mimics. 2013, Patent US9981008B2.
[31] R. Kuai, et al., Synthetic high-density lipoprotein nanodisks for targeted withalongolide delivery to adrenocortical carcinoma, Int. J. Nanomedicine 12 (2017) 6581.
[32] Y. Guo, et al., Perhexiline activates KLF14 and reduces atherosclerosis by modulating ApoA-I production, J. Clin. Invest. 125 (10) (2015) 3819–3830.
[33] C. Subramanian, et al., Synthetic high-density lipoprotein nanoparticles: a novel therapeutic strategy for adrenocortical carcinomas, Surgery 159 (1) (2016) 284–295.
[34] J. Tang, et al., Effect of size and pegylation of liposomes and peptide-based synthetic lipoproteins on tumor targeting, Nanomedicine 13 (6) (2017) 1869–1878.
[35] G.M. Anantharamaiah, D. Goldberg, Apolipoprotein Mimetics in the Management of Human Disease, Springer, 2015, pp. 29–40.
[36] R. Kuai, et al., High-density lipoproteins: nature's multifunctional nanoparticles, ACS Nano 10 (3) (2016) 3015–3041.
[37] S.A. Didichenko, et al., Enhanced HDL functionality in small HDL species produced upon remodeling of HDL by reconstituted HDL, CSL112: effects on cholesterol efflux, anti-inflammatory and antioxidative activity, Circ. Res. 119 (6) (2016) 751.
[38] D. Li, et al., Effect of synthetic high density lipoproteins modification with polyethylene glycol on pharmacokinetics and pharmacodynamics, Mol. Pharm. 15 (1) (2017) 83–96.
[39] J. Tang, et al., Influence of route of administration and lipidation of apolipoprotein AI peptide on pharmacokinetics and cholesterol mobilization, J. Lipid Res. 58 (1) (2017) 124–136 (p. jlr. M071043).
[40] A. Schwendeman, et al., The effect of phospholipid composition of reconstituted HDL on its cholesterol efflux and anti-inflammatory properties, J. Lipid Res. 56 (9) (2015) 1727–1737 (p. jlr. M060285).
[41] S. Behzadi, et al., Protein corona change the drug release profile of nanocarriers: the "overlooked" factor at the nanobio interface, Colloids Surf. B: Biointerfaces 123 (2014) 143–149.
[42] N. Bertrand, et al., Mechanistic understanding of in vivo protein corona formation on polymeric nanoparticles and impact on pharmacokinetics, Nat. Commun. 8 (1) (2017) 777.
[43] K. Ichikawa, et al., Antiangiogenic photodynamic therapy (PDT) using Visudyne causes effective suppression of tumor growth, Cancer Lett. 205 (1) (2004) 39–48.
[44] S. Tenzer, et al., Rapid formation of plasma protein corona critically affects nanoparticle pathophysiology, Nat. Nanotechnol. 8 (10) (2013) 772.
[45] S.D. Wright, C.L. Shear, CSL112 enhances biomarkers of reverse cholesterol transport after single and multiple infusions in healthy subjects, Arterioscler. Thromb. Vasc. Biol. 34 (9) (2014) 2106–2114.
[46] N. Levin, et al., Macrophage liver X receptor is required for antiatherogenic activity of LXR agonists, Arterioscler. Thromb. Vasc. Biol. 25 (1) (2005) 135–142.
[47] S. Gadde, et al., Development of therapeutic polymeric nanoparticles for the resolution of inflammation, Adv. Healthc. Mater. 3 (9) (2014) 1448–1456.
[48] X.Q. Zhang, et al., Nanoparticles containing a liver X receptor agonist inhibit inflammation and atherosclerosis, Adv. Healthc. Mater. 4 (2) (2015) 228–236.
[49] Z.G. Ouedraogo, et al., Role of the liver X receptors in skin physiology: putative pharmacological targets in human diseases, Chem. Phys. Lipids 207 (2017) 59–68.
[50] S. Zheng, et al., Activation of liver X receptor protects inner retinal damage induced by N-methyl-D-aspartate, Invest. Ophthalmol. Vis. Sci. 56 (2) (2015) 1168–1180.
[51] A. Katz, et al., Safety, pharmacokinetics, and pharmacodynamics of single doses of LXR-623, a novel liver X-receptor agonist, in healthy participants, J. Clin. Pharmacol. 49 (6) (2009) 643–649.
[52] Effects of CS-8080 in Healthy Volunteers, Available from: https://clinicaltrials.gov/ct2/show/NCT00613431, 2008.
[53] Multiple-dose Study to Evaluate the Safety, Pharmacokinetics and Pharmacodynamics of BMS-779788 in Healthy Subjects, Available from: https://clinicaltrials.gov/ct2/show/NCT00836602, 2011.
[54] A Safety Study of BMS-852927 in Subjects With Hypercholesterolemia, Available from: https://clinicaltrials.gov/ct2/show/NCT01651273, 2013.